J Mater Sci (2008) 43:3338–3350
DOI 10.1007/s10853-008-2484-6

Accelerated weathering behavior of poly(phenylene ether)-based TPE

Samik Gupta · Tapan Chandra · Arun Sikder · Ashok Menon · Anil K. Bhowmick

Received: 18 November 2007 / Accepted: 18 January 2008 / Published online: 21 March 2008

Abstract In this report accelerated weathering characteristics of a novel poly(phenylene ether) (PPE)-based thermoplastic elastomer (TPE), i.e. a blend of styrene–ethylene–butylenes–styrene (SEBS)/ethylene vinyl acetate (EVA) and PPE-polystyrene (PS), were studied in detail. Exterior and interior accelerated weathering protocols were followed during photooxidative weathering to simulate outdoor and indoor (behind window glass) applications, respectively. Photooxidative degradation was monitored through optical and mechanical property measurements on the injection molded TPE. The effects of titanium dioxide and carbon black at variable loadings were also studied during the photooxidation process. Attempt was made to analyze the surface mechanical properties through nanoscratch/nanoindentation measurement. Using atomic force microscopy, surface roughness and erosion of the exposed material were investigated. Changes in chemical functionalities due to photooxidative degradation were monitored using attenuated total reflection (ATR)-FTIR. Structure property correlation was established through mechanical (surface and bulk), optical, chemical, and morphological analyses.

Introduction

Thermoplastic elastomer (TPE) is a special class of rubbery material, which can be fabricated by techniques usually associated with thermoplastic resins [1]. Thermoplastic elastomeric materials have become important in recent years for their rubbery properties at ambient temperatures and easy melt processibility like thermoplastics [2]. Different TPE systems have been discussed extensively in books by Holden et al. [3] and Bhowmick and Stephens [2]. Recently, Bhowmick et al. [4] reported the development of a series of poly(phenylene ether) (PPE)-based novel TPEs, through twin-screw extrusion and injection molding techniques, which exhibited good mechanical integrity, elastic recovery, stable morphology, and recyclability.

The applications of TPEs cover a wide sector of industries. The range of applications varies from consumer goods, automobiles, wire and cables, appliances, and even sporting goods. Hence, high strength, toughness, mar resistance, and weatherability are the key requirements for such applications [5]. TPEs are qualified for exterior applications after passing through the exterior protocol of the accelerated aging, wherein the material degradation due to exposure to light, humidity, and water is studied. Similarly, indoor application-based materials are examined through an interior accelerated weathering protocol, in which material degradation due to light and temperature behind window glass or indoor application is investigated. With an improved stabilization system, the new generation of styrene block copolymers (SBC) withstands outdoor simulation periods of several years [6]. Polyolefin thermoplastic vulcanizate (TPV or TPE-V) products have been recently developed for application in automotive interiors for low fogging and surface durability, easy to color, fully weatherable, and processable with extrusion–injection molding route [7].

Weathering behavior of various TPEs [8–18] have been studied extensively in recent past. Weathering on thermoplastic polyester elastomers has been studied in detail and the effects of wavelength range of light, temperature, and water

S. Gupta · T. Chandra · A. Sikder · A. Menon
GE India Technology Centre, EPIP Phase II, Whitefield Road, Bangalore 560066, India

A. K. Bhowmick (✉)
Rubber Technology Centre, Indian Institute of Technology (IIT), Kharagpur 721302, India
e-mail: anilkb@rtc.iitkgp.ernet.in

on photodegradation have been reported [9–12]. Superior weathering, oxidative and chemical resistance of the saturated rubbery segments has been achieved by synthesizing triblock TPEs with polyisobutylene (PIB) as centre blocks [13]. It is demonstrated that antioxidants and UV stabilizers aid in enhancing weatherability [14]. Effect of outdoor environment and UV irradiation on styrene acrylonitrile (SAN) copolyester TPE graft polyblends has been reported [15]. Bhowmick and White reported several studies on photodegradation of TPEs based on polyethylene [16–18].

In our earlier communication, the role of ethylene vinyl acetate (EVA) as a compatibilizer, in the quaternary blend, to improve the delamination effect (poor percent elongation at break) was discussed in detail [19]. In this article an effort has been made to understand the weathering performance of the PPE-based novel TPE system (SEBS/EVA/PPE-PS). In the course of developing the domain knowledge of our TPE system, weathering performances of the individual components, i.e. EVA, PPE, polystyrene (PS), and styrene–ethylene–butylenes–styrene (SEBS), have been scrutinized in detail. In the case of photooxidation of EVA, increase in the gel content due to cross-linking reaction was found dominant in EVA's structural change as a consequence of degradation [20]. Several research groups have reported the photooxidative degradation of PPE [21–26]. The photooxidative degradation of SEBS has been studied at wavelengths cutoff below 290 nm, and monochromatic light of 254 and 365 nm, using a variety of spectroscopic methods [27]. The mechanism of photooxidative degradation of PS at low wavelength (usually at 254 and 300 nm) has been discussed in detail [28].

With the understanding of the weathering performances of individual components of the as-developed TPE, the current investigation is aimed to study the cumulative behavior of these components in the accelerated weathering of the quaternary blend of SEBS/EVA/PPE-PS. The degradation due to the exposure to light and temperature often causes a premature failure of optical and mechanical properties of the material. When a material is exposed to weathering conditions, the degradation starts at the surface and slowly propagates into the bulk as a function of time. In the present investigation, initial surface degradation has been exemplified using surface mechanical characterization techniques such as nanoindentation/nanoscratch to characterize the weathering behavior of the blend. This approach is unique and first of its kind for monitoring the weathering of a PPE-based TPE.

Experimental

Materials

The poly(2,6-dimethyl-1,4-phenylene ether) or PPE used in these studies were commercial grade materials which were obtained from GE Plastics, BoZ (Bergen op Zoom), The Netherlands. Intrinsic viscosity (IV in dL g^{-1}) and M_w (g mol^{-1}) of PPE were found to be 0.41 and 4.4×10^4, respectively. General purpose PS (GPPS) with the grade name SC203EL (tensile strength ~47 MPa, percent elongation ~5%, density ~1,050 kg/m^3) was procured from Supreme Petrochemical Ltd., Mumbai, India. SEBS copolymers used in this work were commercial grade material, KRATON®G 1652 (styrene/rubber ~30/70, M_w ~ 7.8×10^4 g mol^{-1}, density ~910 kg/m^3, tensile strength ~31 MPa, percent elongation ~500%), obtained from the KRATON POLYMERS, USA. SEBS is a block copolymer with two glass transition temperatures [~95 °C for the PS blocks and approximately −55 °C for (ethylene/butylene) blocks]. EVA with VA content ~50% [LEVAPREN® 500 (VA content ~50%, M_w ~2.3×10^5 g mol^{-1})] was obtained from Lanxess, Leverkusen, Germany. White pigment titanium dioxide (TiO_2-treated rutile), grade name R103-15 [manufactured by the chloride process; TiO_2—minimum 96 wt.%; alumina—maximum 3.2 wt.%; organic treatment—0.2 wt.% carbon; pH 6.5 (aqueous slurry)] and carbon black, grade name 1333-86 were obtained from DuPont, Wilmington DE 19898, USA.

Preparation of samples (SEBS/EVA/PPE-PS quaternary blend)

PPE/PS was mixed in the ratio of 60/40 by weight. After mixing in a dry mixer, the material was fed into a twin-screw extruder (ZSK 25 from Werner and Pfleiderer, Stuttgart, Germany). The processing temperature was kept in the temperature range 260–270 °C. Extruded PPE/PS granules were mixed with SEBS and EVA and fed into the 10-zone barrel twin-screw extruder with a L/D = 40. Temperature profile for different zones was as follows: 100 °C (Zone 1) to 270 °C (Zone 10) and the temperature of the die was 275 °C. Screw speed was set at 300 rpm (counter-rotating screw) with a throughput rate of 15 kg/h. After extrusion, granules were dried at 70 °C and fed into an injection-molding machine [De-Tech100 LNC4-E (L&T-100T, Chennai, India—screw diameter of 32 mm, L/D ~20)]. Temperature at different zones was set as follows: 270 °C (NOZ); 275 °C (MH3); 260 °C (MH2); 240 °C (MH1); 60 °C (Feed), and 60 °C (Mold). Injection pressure was 50 bar and injection speed was 18 mm/s. Back pressure was 7 bar and total cycle time was kept as 32 s. Tensile test specimen was made complying with ASTM D 412-98a. The samples were duly conditioned (50% humidity at 25 °C for 48 h) prior to testing.

Weathering studies were conducted on SEBS/EVA/PPE-PS (45/30/25) quaternary blends with different loadings of titanium dioxide (TiO_2) and carbon black pigment. Table 1 shows the different formulations exposed in

Table 1 Different formulations exposed in exterior and interior weathering protocols

Samples	EVA (%)	SEBS (%)	PPE-PS (%)	Carbon black (%)	TiO_2 (%)
S1	30	45	25	–	–
S2	30	45	25	–	0.5
S3	30	45	25	–	1
S4	30	45	25	–	1.5
S5	30	45	25	0.25	–
S6	30	45	25	0.5	–

exterior and interior weathering protocols. S1 is the control batch without any pigment along with three batches (S2, S3, and S4) with 0.5, 1.0, and 1.5% TiO_2, respectively. S5 and S6 contain 0.25 and 0.5% carbon black.

Weathering

Weathering exposure was conducted in a Ci5000 Weather-Ometer® from Atlas Material Testing Solutions, USA, following specified weathering test protocols mentioned in Table 2. Modified (Mod) ASTM G155 (exterior application) test standard with high irradiance 0.75 W/m^2 (at 340 nm optical filter to control irradiance) was used for exterior weathering test protocol. The test consisted of continuous light exposure for 120 min (102 min light exposure without spray-cycle 1; and 18 min of light exposure with specimen spray-cycle 2). Sample surface temperature, i.e. black panel temperature (BPT), was 63 °C and the relative humidity (RH) was maintained at 50% on light cycle. This test included an additional segment of water spray in the presence of light exposure to simulate outdoor conditions.

In interior test protocol, ISO4892-2B was followed. The samples were exposed to an irradiation level of 1.15 W/m^2 (at 420 nm optical filter to control irradiance) for 4,000 h. This test consisted of only light exposure without any spray. Sample surface temperature, i.e. BST, was at 63 °C (black standard temperature) along with the same humidity level used for the exterior protocol. The major difference between two test protocols was the inner and outer filter combination. In the case of interior protocol, the outer filter was changed from S borosilicate to Sodalime, which had a cutoff of 310 nm wavelength instead of 285 nm.

Color shift measurement

Color shift was measured using the Color Eye 7000A spectrophotometer from GretagMacbeth. The instrument

Table 2 Weathering test protocols

Parameter	Mod ASTM G155 (G26)	ISO 4892-2B
Total number of segments	2	1
Controlling black sensor	Black panel temp	Black standard temp
Irradiance filter (optical filter) (nm)	340	420
SEG 1: Irradiance wattage (W/m^2)	0.75	1.15
SEG 1: Black sensor temperature (°C)	63	65
SEG 1: Chamber temperature (°C)	42	40
SEG 1: Relative humidity (%)	50	50
SEG 1: Duration	102 min	Continuous light
SEG 2: Irradiance wattage (W/m^2)	0.75	–
SEG 2: Spray type (ON)	Specimen	No spray cycle
SEG 2: Duration (min)	18	–
Inner filter	S′ borosilicate glass	S′ borosilicate glass
Outer filter	S′ borosilicate glass	Soda lime glass
Typical exposure duration (h)	4,000	4,000

settings were done with the "color space" as "CIE Lab", measurement mode SCI–UV included, large lens/large aperture, observer angle 10°, and the illuminant D65 (D65 illuminant was used which is similar to day light spectra). Color of a substrate was represented by using "L", "a", and "b", where "L" is the lightness, "b" is the representation of blue or yellowness and "a" is the representation of green or redness. The color spectrophotometer measured overall color difference between two different samples, which was represented as ΔE. The data were reported on L, a, b scales and overall color difference was given in Eq. 1 [28],

$$\Delta E = \sqrt{(\Delta L)^2 + (\Delta a)^2 + (\Delta b)^2} \quad (1)$$

where $\Delta L = L_2 - L_1$, $\Delta a = a_2 - a_1$, and $\Delta b = b_2 - b_1$.

Respective numbers 1 and 2 are denoted to samples before and after the exposure test.

Spectral distribution data were obtained from color spectrophotometer (using D65 light source) by plotting % reflection (opaque samples) with wavelength of light in nanometers. The color spectrophotometer provides the data from 360 to 760 nm.

Mechanical properties

Tensile tests were carried out in an Instron 3365, Noorwood, USA. Pneumatic grips were used for better gripping. Dumbbells-shaped samples were made complying with ASTM D412-98a. Tensile strength and percent elongation at break were reported at 25 °C, with a deformation rate ~200 mm/min.

Surface mechanical properties—Nanoscratch/ Nanoindentation technique

Nanoscratch testing was performed on the Nanoindenter® XP automated system (MTS Systems Corp., Oak Ridge, TN, USA). The system had an indentation head, which was calibrated with microscope for coordinating the locations to be tested. Indenter head which was load-controlled was applied normal to the sample surface by the magnet/coil system. The resolution of the load and displacement is given in Table 3. Maximum distance allowed for the indenter travel, normal to the sample surface, was about 1.5 mm. Over this entire range, displacement resolution was <0.1 nm. The maximum load capacity for this system was 500 mN with a precision of <1 μN. A typical Berkovich diamond tip having end diameter ~200 nm was used for all scratch experiments.

A typical scratch experiment was performed in four stages: (1) an original profile, (2) a scratch segment, (3) a residual profile, and (4) a cross profile (profile across the scratch length). Due to high percent recovery and surface roughness, the cross profile could not be measured in the current TPE (SEBS/EVA/PPE-PS). Schematic of the first three stages of the procedure used in this study is shown in Fig. 1. In the original profile, surface morphology was obtained by pre-profiling the surface with 50 μN load at a predetermined location where the scratch was to be performed. In the next step the indenter started moving from the initial location and scratch experiment started with an increasing normal load from 50 μN to 5 mN. A post-scratch profile was performed along the same path with 50 μN load to measure the residual deformation in the groove. Test parameters followed in the current nanoscratch test is given in Table 4.

Percent recovery was calculated from the penetration curves during and after scratch. Figure 2 shows a typical

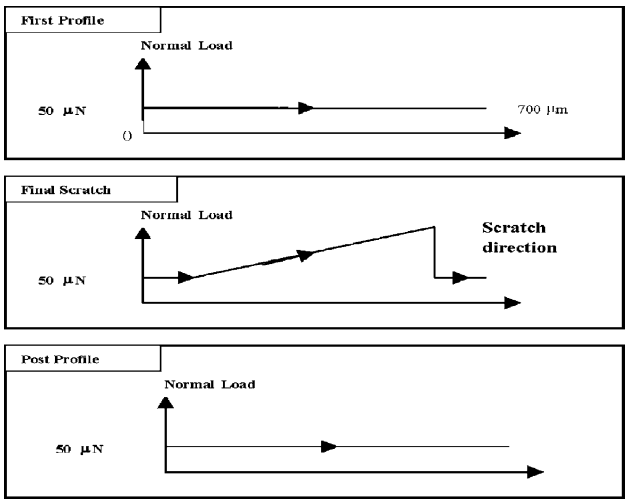

Fig. 1 Three steps in a complete scratch experiment

penetration curves during and after scratch experimentation. Equation 2 was used to calculate percent (%) recovery at a distance 400 μm.

$$\%\text{Recovery} = \frac{\text{Depth}_1 - \text{Depth}_2}{\text{Depth}_1} \times 100 \quad (2)$$

Nanoindentation was also performed on the sample surfaces in order to find the change in surface mechanical properties like hardness and modulus on the exposed samples. As rubber samples are highly elastic in nature with high recovery, it is not possible to calculate numerical values for hardness and modulus. Instead efforts were made to understand change in surface property through analysis of loading and unloading curves. Indentation experiment was performed using constant strain rate of 0.05 s^{-1}.

Atomic force microscopy

Atomic force microscopy (AFM) study was done to estimate the surface roughness generated owing to accelerated weathering of this blend. AFM studies were carried out in air at ambient conditions (25 °C, 60% RH) using a multimode Atomic Force Microscope from Digital Instruments Inc., Santa Barbara, CA, USA. Topographic (height) and phase (phase contrast) images were recorded in the tapping mode (TMAFM) attached with a Nanoscope IIIa feedback controller, equipped with a Nanoscope Extender Ex-1 module. Phase images were captured in tapping mode

Table 3 Specifications of the Nanoindenter® XP system

Maximum applied load (mN)	Displacement resolution (nm)	Max indentation depth (μm)	Load resolution (nN)	Damping coefficient (Ns)	Resonant frequency (Hz)
500	<0.1	75	50	2	20

Table 4 Scratch parameters used in the current study

Maximum load	Scratch velocity	Scratch length	Profile load	Tip	% Recovery at a distance
5 mN	10 μm/s	500 μm	50 μN	Berkovich type (~0.2 mm dia)	400 μm

using etched silicon probe tips (LTESP). Its higher nominal spring constant (48 Nm^{-1}) ensures the proper scanning of all the hard and soft segments in the blend in the present study. A cantilever length of 225 μm ensures proper scanning by the probe in the intricate parts on the surface of the blend. For each sample, three or more images were analyzed. The cantilever was oscillated at its resonance frequency (ω_0) of ~170 kHz. Images were recorded with the set point ratio ($r_{sp} = A_{sp}/A_0$, where A_0 = free oscillation amplitude and A_{sp} = set point amplitude selected for the measurement) of 0.8–0.9. All the images were collected with the 512 pixels in each direction (x, y). The scan direction was rotated to ensure the proper morphology detected by the AFM tip. Roughness was calculated by drawing line across the images.

Attenuated total reflection (ATR)-FTIR

All the attenuated total reflection (ATR)-FTIR spectra were obtained by using Di-ATR probe with two reflectors manufactured by Specac Inc., Kent, UK. Diamond crystal was used as the internal reflectance element. This accessory was attached to Perkin Elmer Spectrum GX FTIR spectrophotometer connected to SPECTRA software from Perkin Elmer. The spectrophotometer was purged with N_2 gas to reduce the effects of CO_2 absorption in its optical path. Ratio method was applied to each spectrum, wherein the background recorded in air was automatically subtracted. This method reduced the signal to noise ratio. Sixty-four scans were done for each sample.

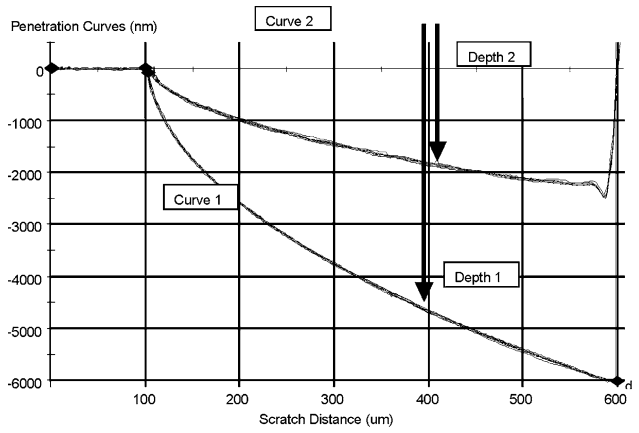

Fig. 2 Penetration curves during scratch testing. Curve 1 represents the depth of indenter during scratch with increasing load and curve 2 represents the depth after ~1 min of scratch

Results and discussion

Color shift due to weathering

The effect of photooxidative degradation of novel PPE-based TPE simulating both exterior (outdoor application) and interior (behind window glass application) protocols are reflected on optical properties. In this study, the irradiation starts after 285 nm for exterior test cycle. Figure 3a, b shows the color shift, ΔE, by exposing the test specimens to accelerated weathering conditions (exterior and interior) for different time intervals (0, 250, 500, 750, 1,000, 1,500, 2,000, 2,500, 3,000, and 4,000 h). Prominent color shift was observed in TiO_2-containing samples (S2–S4) as well as in control sample (S1) after initial exposure (250 h), except the samples containing carbon black (S5 and S6). Here carbon black itself was acting as a UV absorber. In Fig. 3a, S2–S4 shows an initial increase in ΔE

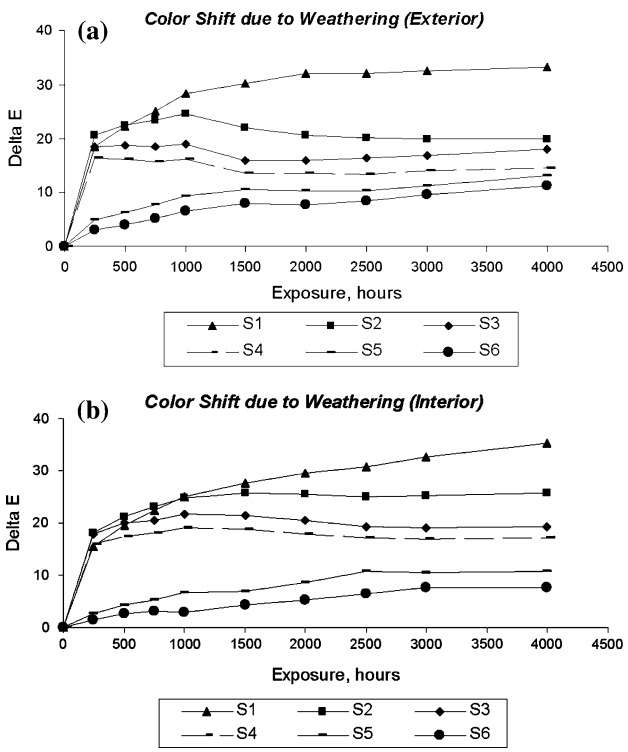

Fig. 3 Change in color, ΔE, for (**a**) exterior and (**b**) interior protocols

by ~20% at 250 h of exposure. Beyond 250 h, the change in color is found to be insignificant. These batches (S2–S4) lose the surface gloss by the degradation of the polymeric part followed by an increase in concentration of pigment on the surface [28]. This led to stabilization of change in color on further prolonged exposure up to 4,000 h. The effect of pigment loading was observed with the samples containing carbon black and TiO_2. Keeping the type of pigments fixed, incorporation of more pigment reduces the overall color shift. We have observed a similar color shift behavior in the "interior test" of the exposed samples, as shown in Fig. 3b. It was reported that PPE showed a very significant ΔE shift (>4.8) after 200 h of interior weathering exposure [29]. This combined effect of photooxidative degradation is also reflected in spectral distribution data of the control sample (S1). Prominent absorption of light at the UV region (300–400 nm) as well as visible region was observed. Irrespective of test protocols, percent reflection data shows (Fig. 4) a significant drift in spectral distribution at 250 h of external exposure, which increases with prolonged exposure. Beyond 2,000 h of exposure this drift is found to be insignificant. This phenomenon also supports the color shift behaviors (refer Fig. 3a, b). The color shift can be attributed to the change in chemical functionalities owing to degradation, which has been addressed in the subsequent ATR-FTIR section.

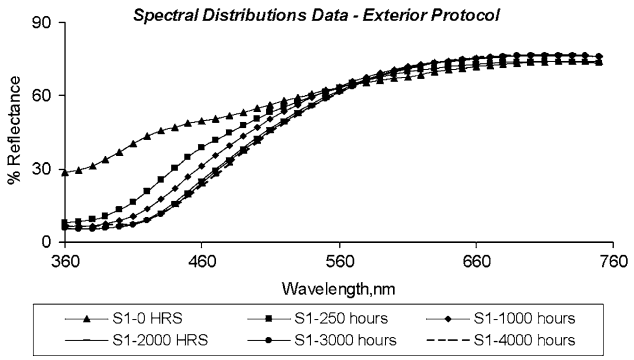

Fig. 4 Spectral distribution data for S1 in exterior protocol

Change in mechanical properties upon weathering

Mechanical property measurements like tensile strength and elongation at break were performed after exposing the test specimens to accelerated weathering conditions for following different time intervals viz. 0 (unexposed), 250, 500, 1,000, 1,500, and 4,000 h. Table 5 registers the values of tensile strength and percent elongation at break for all the batches (S1–S6) for the exterior exposure. Figure 5a–d shows the effect of external and internal accelerated weathering on few representative samples of TPE containing TiO_2 (S4) and carbon black (S6) along with S1 (the batch without any pigment). It is noteworthy that in the exterior exposure, the control batch, S1 shows significant drop (~29%) in elongation at break at 500 h of exposure (Fig. 5a, b). Drop in tensile strength and percent elongation at break for S1 has reached the maximum at 1,000 h of exposure and attains a plateau. However, following Table 5, the extent of fall of mechanical properties reduces with increase in amount of the pigments, which mainly act as a UV stabilizer. Similar effect is also observed with S5 and S6 (containing carbon black pigment, 0.25 and 0.5% ppw, respectively). In general, the maximum decrement in mechanical properties is observed with S1 (the control sample), which is manifested by ~33% drop in tensile

Table 5 Tensile strength and percent elongation at break of the quaternary blend following exterior weathering protocols

Exposure (h)	S1	S2	S3	S4	S5	S6
Tensile strength (MPa)						
0	18.94 (0.13)	18.07 (0.89)	18.20 (0.50)	18.50 (0.40)	18.20 (0.50)	18.27 (0.34)
250	18.76 (0.71)	19.20 (0.54)	19.00 (0.45)	19.46 (1.13)	16.44 (0.74)	18.50 (0.46)
500	16.05 (0.46)	15.80 (1.16)	17.60 (0.28)	18.33 (0.32)	15.70 (1.20)	17.02 (0.89)
1000	12.87 (1.10)	14.46 (0.56)	17.17 (0.84)	16.92 (0.27)	14.40 (0.50)	16.84 (0.78)
1500	12.42 (0.09)	14.15 (0.43)	16.15 (1.10)	16.50 (0.21)	14.30 (1.30)	17.00 (0.30)
4000	12.68 (0.29)	13.62 (0.54)	15.50 (0.88)	16.30 (0.70)	13.71 (0.43)	15.90 (0.86)
Elongation at break (%)						
0	192 (8)	170 (18)	158 (19)	171 (13)	194 (12)	195 (2)
250	188 (7)	175 (2)	164 (3)	164 (25)	144 (10)	179 (1)
500	137 (11)	121 (15)	142 (7)	148 (11)	128 (9)	150 (8)
1000	88 (12)	115 (11)	135 (12)	134 (6)	110 (5)	146 (10)
1500	78 (3)	109 (2)	114 (27)	136 (2)	113 (9)	155 (11)
4000	80 (3)	118 (3)	117 (12)	135 (13)	110 (9)	132 (7)

Note: Standard deviations are mentioned in parenthesis

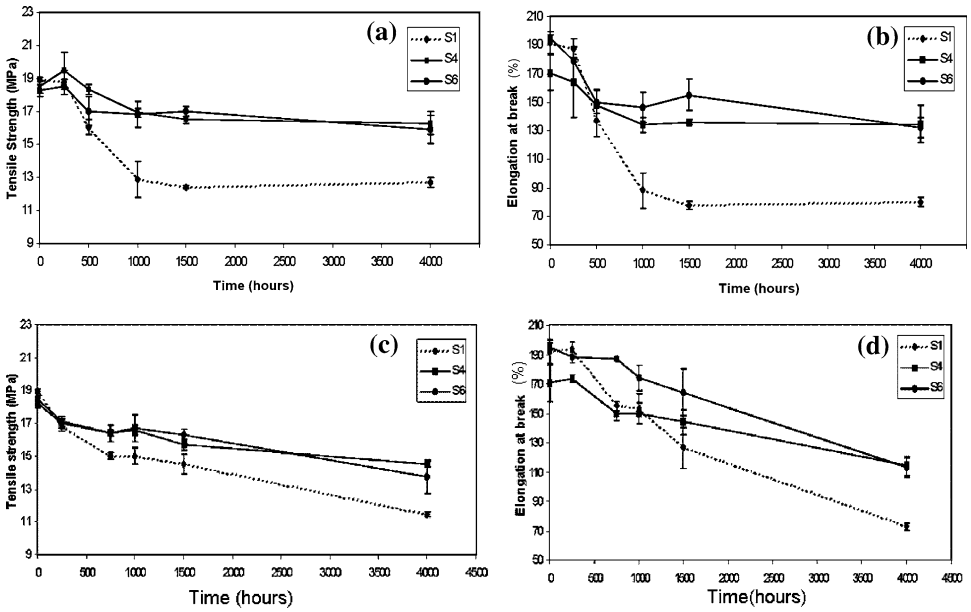

Fig. 5 Tensile strength and percent elongation at break in exterior protocol (**a** and **b**) and in interior protocol (**c** and **d**)

strength and ~59% drop in percent elongation at break after 4,000 h of exposure. Similarly, in Fig. 5c, d, drop in tensile strength and percent elongation at break is observed for the samples exposed following the interior protocol. Main difference observed during exterior and interior protocol is the rate at which the mechanical properties dropped due to weathering exposure. The rate of degradation is slower in interior protocol compared to that in exterior protocol. The color shift was significantly less in the samples containing carbon black (acts as UV absorber) compared to those containing white (TiO_2) pigment. However, in mechanical properties, like tensile strength and elongation at break, which represent the bulk characteristics of the material, the performance of the quaternary blend is similar with both the pigments. For example, in Table 5, similar drop in tensile strength and percent elongation at break is observed in S2 and S5 after 4,000 h of exterior exposure.

Thus, the optical and mechanical properties, upon weathering of SEBS/EVA/PPE-PS quaternary blends, depend on the type and quantity of the pigment in the system. Further effort has been made to develop a detailed understanding on optical/mechanical properties with the chemical and structural development of the blend, including a detailed study on the surface morphology and surface mechanical properties of the blend (sections "Surface mechanical properties", "Atomic force microscopy", and "ATR-FTIR spectra—chemical evidence of degradation"). S5 with 0.25% carbon black has been selected as a representative batch to understand the detailed structure property correlation upon accelerated weathering.

Surface mechanical properties

Impression of the scratch (created by Nanoindenter® XP) on the surface along with the change in surface morphology due to weathering is shown in Fig. 6. Sharp and thin scratch is observed on the unexposed sample (Fig. 6a). Due to weathering, the nature of the scratch has changed and has become wider (Fig. 6b, c). This effect of broadening of scratches is the manifestation of degradation on the surface. The effect of degradation leads to change in the nature of the surface as it became more brittle leaving only the pigmented portion of the material on the surface [28]. With further exposure in accelerated weathering, the surface roughness increases by a significant amount (Fig. 6 d, e), which is discussed in the section "Atomic force microscopy". Increase in roughness owing to degradation results

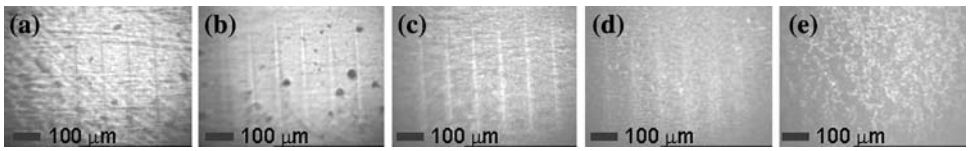

Fig. 6 Optical micrographs show scratch impressions for S5 (exterior protocol) with different exposure time (**a**) 0 h, (**b**) 500 h, (**c**) 1,000 h, (**d**) 1,500 h, and (**e**) 4,000 h

in poor visibility of the scratches on the sample surface (Fig. 6d, e).

In the area of surface mechanical properties, nanoscratch measurement is usually done in thermoplastic material with hard and smooth surface. Due to high surface roughness and soft elastic nature of the PPE-based TPE, measurement of scratch dimension could not be done from the nanoscratch measurement. A unique approach is adopted to calculate the change of percentage recovery from the penetration curves (refer Fig. 2). In Fig. 7, an attempt has been made to correlate percent recovery with exposure time, which is derived from penetration curves of S5 exposed for different period of time. Decrease in percent recovery is an indication of surface brittleness due to degradation.

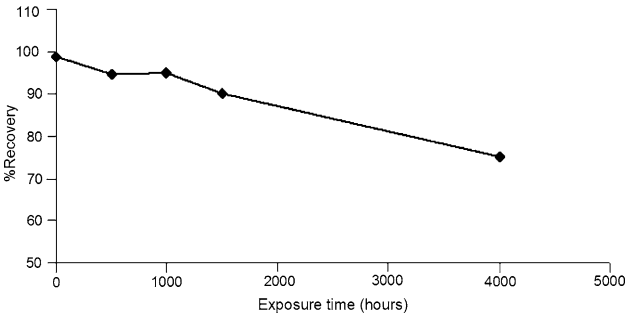

Fig. 7 Change in percent recovery for S5 with exterior exposure time (hours) in nanoindentation measurement

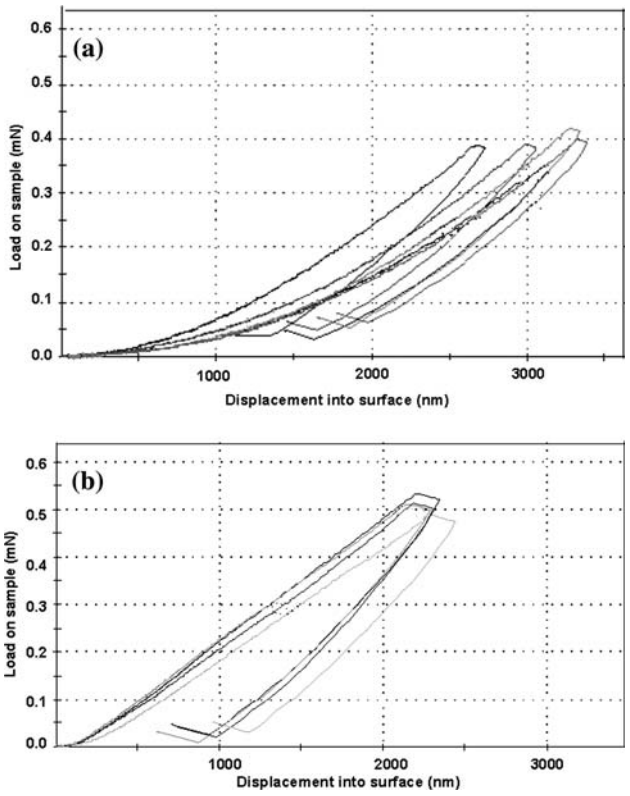

Fig. 8 Loading–unloading curves generated on the S5 sample surfaces with nanoindentation (**a**) unexposed and (**b**) exposed for 1,500 h

Thus the effect of weathering on surface and bulk mechanical property has been observed as a function of exposure time. As in weathering, degradation starts from the surface, percent recovery calculated from nanoscratch technique can be a viable method of characterizing mechanical performance of material during weathering. In order to investigate the surface hardness change, nanoindentation loading–unloading curve (Fig. 8) is generated on S5 samples (exposed and unexposed). Change in nature of loading–unloading curves with exposure time is an indication of loss of elastomeric properties upon weathering. In the unexposed sample, loading–unloading traces are with radius of curvature higher than those for exposed samples. Moreover, exposed sample requires nearly twice the load for achieving a similar amount of penetration depth compared to that for unexposed one. Nanoindentation and scratch at low load regime have not been tried on studied TPE due to highly elastic and soft nature. This study clearly shows that this technique can be used to characterize small change in surface mechanical properties upon accelerated weathering.

Atomic force microscopy

Three-dimensional height image (Fig. 9a) and corresponding phase image (Fig. 9b) of the unexposed S5 sample shows a reasonably smooth surface. The z range of the 3D image has been kept constant at 1.0 μm. This gives a clear indication that the initial sample surface was reasonably smooth having root mean square (RMS) roughness (R_{rms}) and arithmetic roughness (R_a) in the range of 10–30 nm and 10–20 nm, respectively, for the entire image. Upon weathering for 1,000 h, surface irregularities are observed, as shown by the 3D height image and corresponding phase image (Fig. 10a, b respectively). Hills and valleys are generated on the surface and R_{rms} and R_a roughness values are found to be in the range of 20–55 nm and 20–40 nm, respectively, upon weathering for 1,000 h following exterior protocol.

Figure 11a, b shows significant damage on the surface by exposing the sample (S5) in accelerated weathering for 4,000 h. From the height image (3D) and associated 2D phase image R_{rms} is found to vary between 100 and 200 nm and R_a between 60 and 110 nm with the same z-range of 1 μm. Generation of very high roughness becomes visibly clear for these weathered samples. In general, Fig. 10 depicts the initiation of progressive damage while Fig. 11 confirms the damaged rough surface of the exposed sample as a consequence of prolonged weathering.

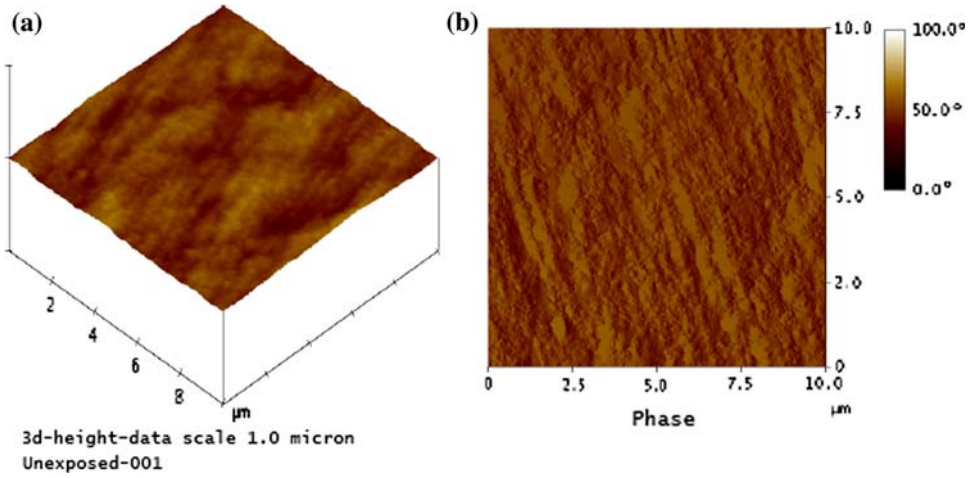

Fig. 9 AFM phase images for unexposed sample of S5: (**a**) surface view and (**b**) planar view

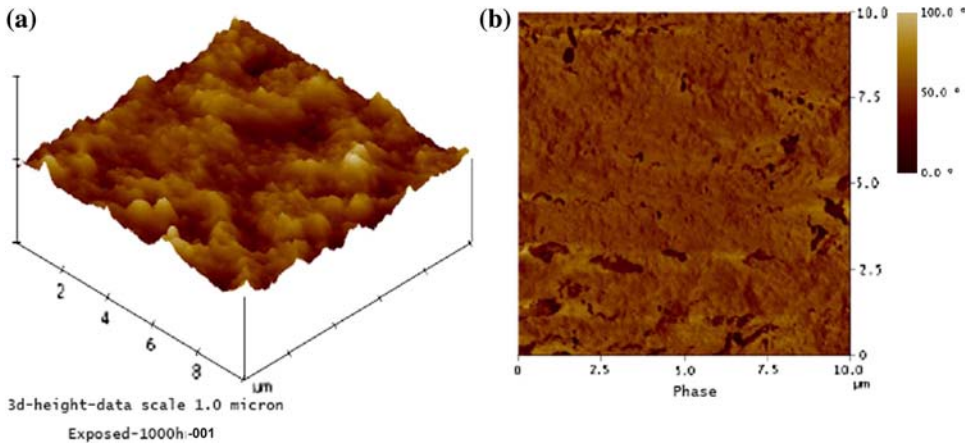

Fig. 10 AFM phase images for 1,000 h exposed (exterior protocol) sample of S5: (**a**) surface view and (**b**) planar view

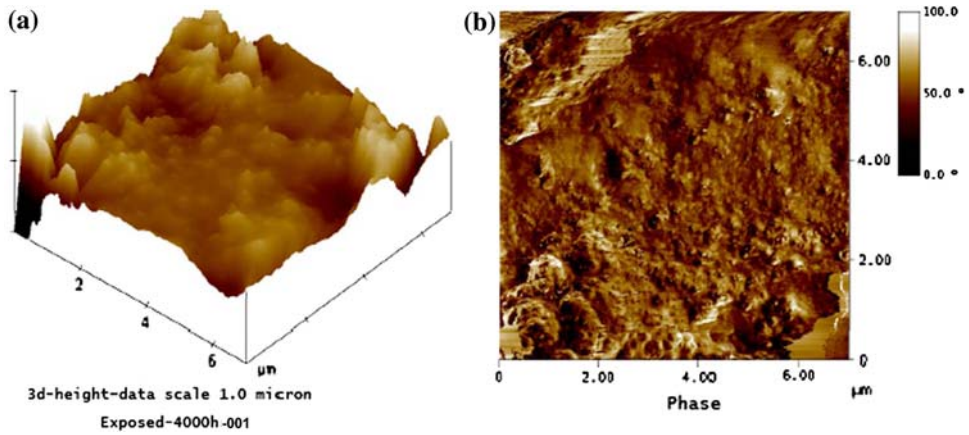

Fig. 11 AFM phase images for 4,000 h exposed (exterior protocol) sample of S5: (**a**) surface view and (**b**) planar view

ATR-FTIR spectra—chemical evidence of degradation

Figure 12 shows representative ATR-FTIR spectra of the controlled (unexposed) sample, S1. Important peaks and their assignments are given in Table 6.

ATR-FTIR study was carried out in S5 for different times of external exposure (0 h—unexposed; 250, 750, 1,000, 1,500, and 4,000 h). Figure 13a shows ATR-FTIR spectra of S5, exposed for different weathering times for the specific region 3,700–2,700 cm^{-1}. The formation of OH functionalities ($\sim$3,400 cm^{-1}) could be arising from degradation of one or more components of the blend (mainly EVA). Percent (%) transmittance at $\sim$3,400 cm^{-1} at each specific time of exposure is calculated from

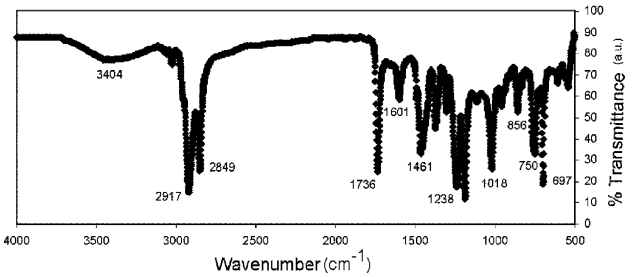

Fig. 12 ATR-FTIR spectra of S1 (unexposed)

Table 6 ATR-FTIR peak assignments and observations

Frequencies (cm^{-1})	Assignments and observations
~697	Out of plane C–H groups in the aromatic ring
~720	Aliphatic C–H bending vibrations from SEBS/PS
~750	Deformation vibration of C–H groups in aromatic ring
~1018	C–C stretch from PS unit
~1186	Characteristic peak for PPE
~1238	C–O–C stretch from PPE/EVA
~1305	Methylene wagging deformation
~1373	Symmetric methyl bending vibrations EVA
~1461	Asymmetric methyl bending vibration
~1601	PS unit
~1736	C=O symmetric stretch
~2849	Symmetric methylene stretch
~2917	Asymmetric methylene stretch
~3404	–OH functionality

Fig. 13a and plotted in Fig. 13b. The decrease in percent transmission with exposure time indicates more significant degradation upon prolonged exposure.

Figure 13c shows the ATR-FTIR spectra of the samples at different exposures for the specific region, 1,300–1,900 cm^{-1}. It is observed that the peak at 1,736 cm^{-1} (due to C=O group) broadens beyond 250 h of exposure. Simultaneously, a peak at 1,650 cm^{-1} appears plausibly due to C=C development as a consequence of deacetylation of EVA present in the studied blend [20]. The peak at 1,305 cm^{-1} disappeared after exposure, indicating that the C–O–C bond in PPE might have broken down due to weathering as well as due to reduction of C–O–C linkage in EVA owing to deacetylation.

The other peaks due to PPE and PS in the region of 800–1,300 cm^{-1} (Fig. 13d) have broadened, indicating the degradation of PPE and PS. Characteristic peak of PPE at 1,186 cm^{-1} is found to disappear after 250 h of exposure. All these results clearly indicate that the accelerated weathering for 250 h and onwards leads to chemical degradation of EVA, PPE, and PS.

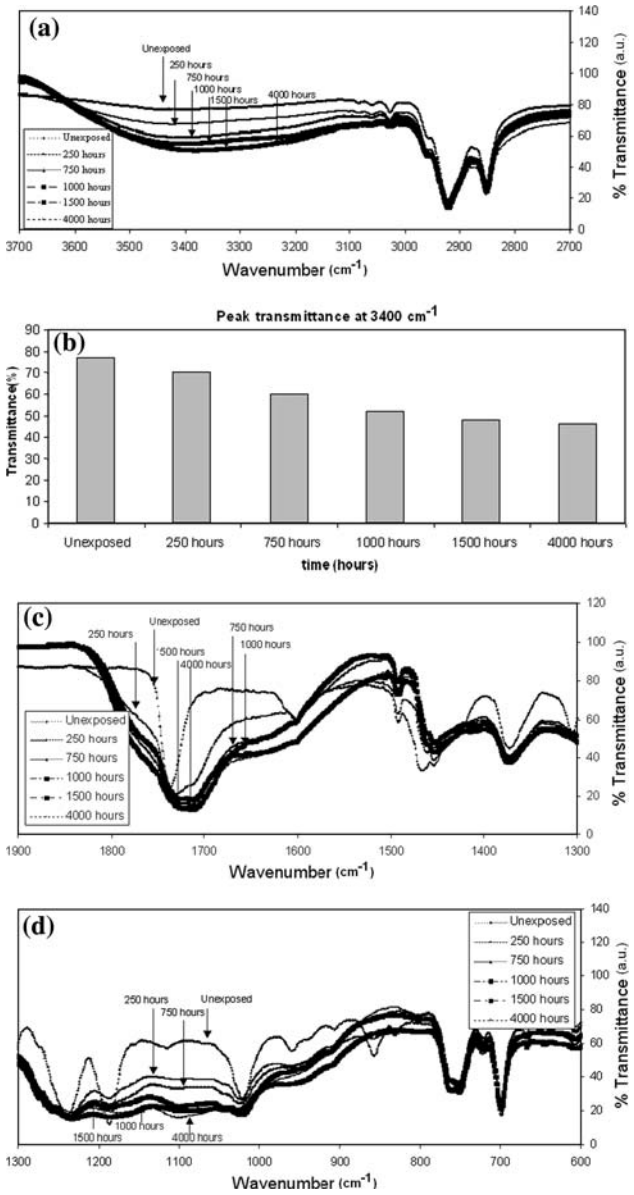

Fig. 13 ATR-FTIR spectra of S5, upon accelerated weathering in exterior protocol: (**a**) 2,700–3,700 cm^{-1}, (**b**) at 3,400 cm^{-1}, (**c**) 1,300–1,900 cm^{-1}, and (**d**) 600–1,300 cm^{-1}

These chemical changes in S5 correlate with our observation in color change of the quaternary blend along with the drop in mechanical properties. The change in chemical functionality upon weathering of individual components of SEBS/EVA/PPE-PS quaternary blend is also monitored to compare and contrast the weathering performance with the quaternary blend. Individual components have been intentionally weathered up to 2,000 h in exterior protocol. Figure 14a–d shows the IR spectra of both exposed and unexposed PPE, PS, EVA, and SEBS respectively.

Figure 14a shows the IR spectra of exposed and unexposed PPE. Several peaks in the region of 800–1,300 cm^{-1} show change in peak pattern and intensity as a manifestation of PPE degradation. The mechanism of degradation of PPE was reported by several groups [21, 25, 26]. The photochemical process as shown in Scheme 1 has been attributed to the formation of benzylic-type radicals by photolytic elimination of oxygen atom [25]. Pickett [21] suggested a self-sensitized photo-induced electron transfer leading to oxidation of polymer backbone generating chain sessions and a large amount of yellowish product (Scheme 2). Rivaton and Morel [26] suggested the photooxidation mechanism under accelerated conditions at both short and long wavelengths as shown in Scheme 3.

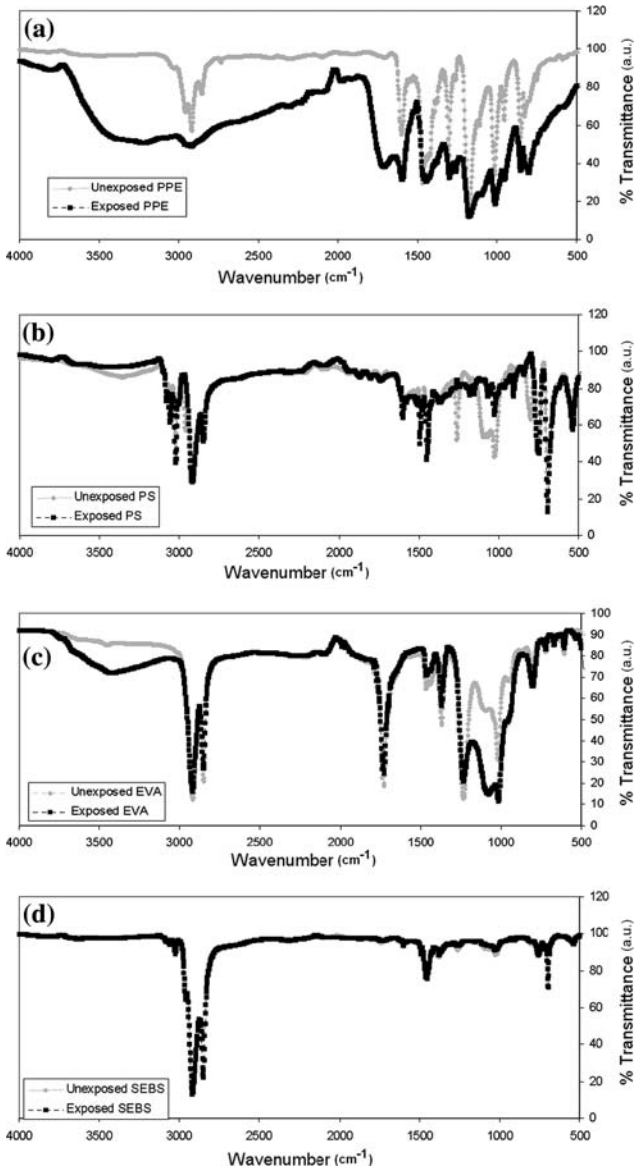

Fig. 14 Unexposed and exposed (exterior protocol—2,000 h exposed) ATR-FTIR spectra of (**a**) PPE, (**b**) PS, (**c**) EVA, and (**d**) SEBS

In the case of PS, for both exposed and unexposed spectra (Fig. 14b), a difference is found (at ~1,020 cm^{-1}) due to "C–C stretch from the PS unit". Moreover, it is reported that degradation of PS depends on the wavelength of the exposed light. Performance at a low wavelength usually at 254 and 300 nm was discussed in detail [28]. It is noteworthy to mention that similar difference in the exposed quaternary blend of SEBS/EVA/PPE-PS is also observed in the region of 800–1,300 cm^{-1}, for the degradation of PPE and PS after 250 h of exposure in the exterior protocol.

Figure 14c shows the photooxidative degradation of EVA compared to the unexposed pure EVA. Difference in transmittance is observed in the zone of 1,000–1,234, 1,374, 1,736, and finally ~3,400 cm^{-1}. Similar behavior is observed in the quaternary blend upon degradation due to accelerated weathering. In fact, prolonged weathering could result in the yellow to brown color in the EVA due to formation of polyconjugated $(C=C)_n$ double bonds of various lengths. Acetic acid and other volatile organic components are also produced due to photochemical decomposition of the EVA [20].

SEBS degradation is found to be minimal. This fact was ascertained by running a simulated weathering experiment on pure SEBS, where no significant changes were noticed in FTIR-ATR (Fig. 14d). FTIR spectra of photooxidized SEBS sample show a predominant absorption associated with carboxylic acids and/or aliphatic esters at 1,712 cm^{-1} [27]. This phenomenon cannot be accounted in our exposed quaternary blend plausibly due to the overlap of other chemical functionality upon weathering. It is noteworthy to mention that the photodegradation of the individual components of the quaternary blend of SEBS/EVA/PPE-PS is reflected on the cumulative response of the PPE-based TPE upon prolonged exposure in our studied accelerated weathering conditions.

Conclusions

Accelerated weathering following both exterior and interior protocol simulated the application perspective of the studied PPE-based TPE. Carbon black prevented significant color shift due to their UV absorption mechanism. In TiO_2 and carbon black containing batches, the level of degradation was found to be dependent on the quantity of pigments. Change in mechanical properties was found to be independent of the type of pigments upon weathering exposure. Due to much more stringent conditions in exterior protocol, faster drop in mechanical properties was

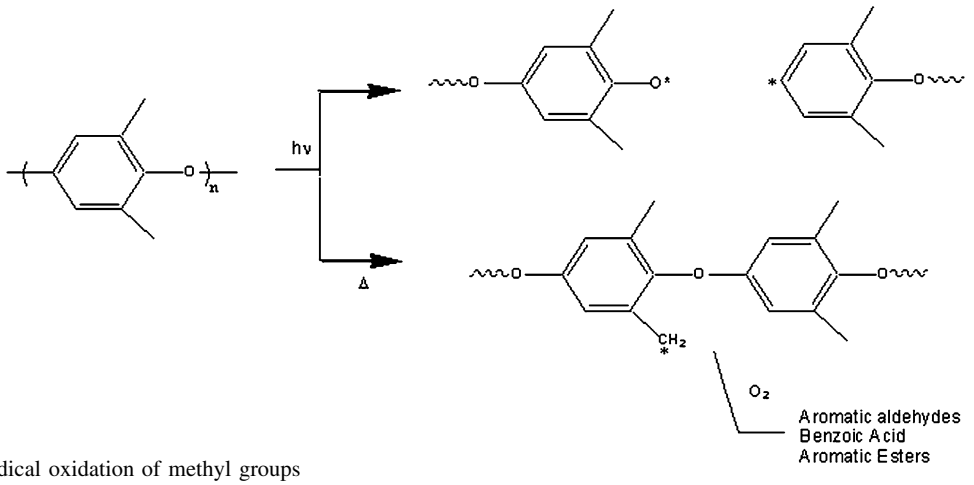

Scheme 1 Free radical oxidation of methyl groups

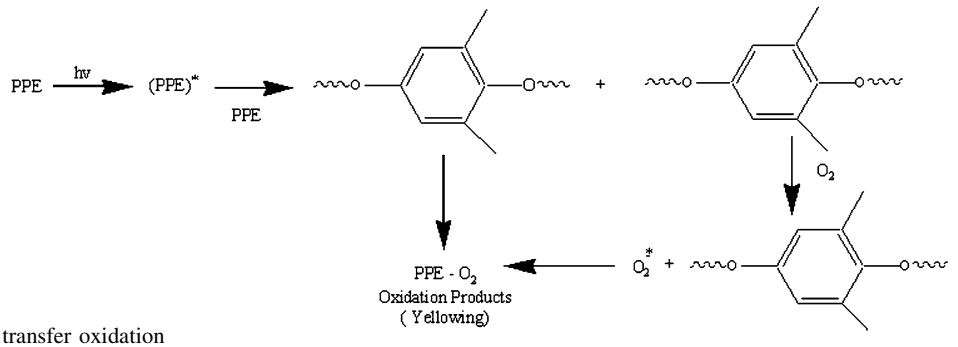

Scheme 2 Electron transfer oxidation

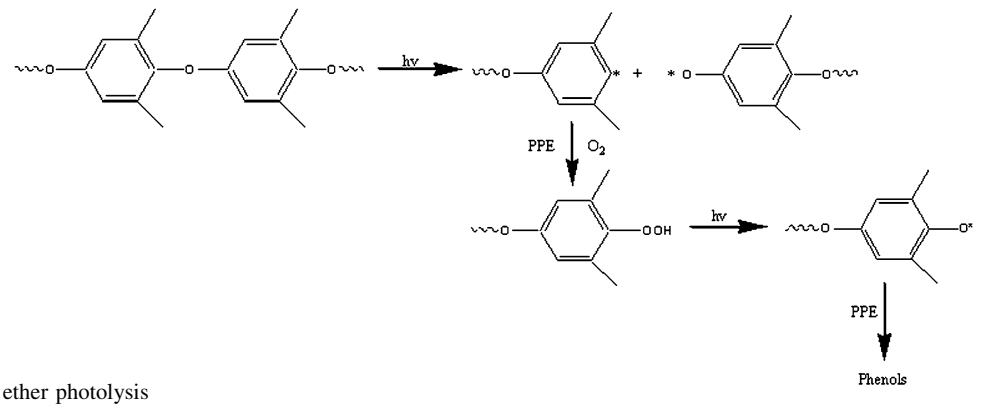

Scheme 3 Direct ether photolysis

found compared to that of internal protocol. The role of pigments as an UV absorber is evident by observing the higher extent of photodegradation and decreased mechanical properties of the control batch (S1) compared to those with pigmented batches. ATR-FTIR studies showed prominent degradation of EVA, PPE, and PS beyond 250 h of accelerated weathering exposure (in exterior protocol). The chemical evidence of degradation was found to be in line with the color shift of SEBS/EVA/PPE-PS along with the drop in mechanical properties. Percent recovery calculations indicated the enhancement of brittleness on the surface due to weathering. Different load–displacement curves through nanoindentation measurement showed the increase in load to achieve a specific penetration in the material with prolonged weathering exposure. AFM studies confirmed the increase in surface roughness of the material upon exposure. Consistent increase in surface roughness (R_{rms} and R_a) value was observed with prolonged accelerated weathering, which indicates surface erosion of the pigmented sample.

Acknowledgements The authors acknowledge GE India Technology Centre and IIT Kharagpur for this joint venture. The authors also thank Drs. Susanta Mitra, Radha Kamlakaran, and Sweta Hegde, and Mr. Anirban Ganguly for their effort.

References

1. De SK, Bhowmick AK (eds) (1990) Thermoplastic elastomers from rubber – plastic blends. Ellis Horwood, London
2. Bhowmick AK, Stephens HL (eds) (2001) Handbook of elastomers, 2nd edn. Marcel Dekker Inc., New York
3. Holden G, Legge NR, Quirk RP, Schroeder HE (1996) Thermoplastic elastomers: a comprehensive review, 2nd edn. Hanser, Munich
4. Bhowmick AK, Gupta S, Biswas A, Preschilla N, Krishnamurthy R (2006) US Patent file number GP2-0448/201393-1: filed on 6th June
5. Wehrenberg RH (1979) Mater Eng (Cleveland) 90:40
6. Gerhard B, Markus BK (2000) Plast Eur 90:42
7. Reid CG, Cai KG, Tran H, Nobert V (2004) KGK-Kautschuk und Gummi Kanststoffe 57:227
8. Lonnberg V, Starck P (1997) Polym Test 16:133
9. Nagai Y, Ogawa T, Nishimoto Y, Ohishi F (1999) Polym Degrad Stab 65:217
10. Jiang-Qing P, Jie Z (1992) Polym Degrad Stab 36:65
11. Tabankia MH, Philippart JL, Gardette JL (1985) Polym Degrad Stab 12:349
12. Tabankia MH, Gardette JL (1987) Polym Degrad Stab 19:113
13. Kennedy JP, Joseph K (1990) Proceedings of the ACS Division of Polymeric Materials Science and Engineering 63:371
14. Chuck ML, Patel S, Farber AJ (1983) Annual Technical Conference—Society of Plastics Engineers 35
15. John CF, Van Fleet V (1992) J Appl Polym Sci 44:1685
16. Bhowmick AK, Ray S, Shanmugharaj AM, Heslop J, Köppen N, White JR (2006) J Appl Polym Sci 99:150
17. Bhowmick AK, Heslop J, White JR (2002) J Appl Polym Sci 86:2393
18. Bhowmick AK, White JR (2002) J Mater Sci 37:5141
19. Gupta S, Biswas A, Preschilla N, Krishnamurthy R, Bhowmick AK (2007) Rubber Chem Technol 80:642
20. Pern FJ, Czanderna AW (1992) Sol Energy Mater Sol Cells (The Netherlands) 25:3
21. Pickett MCR (1990) In: Scott G (ed) Mechanisms of polymer degradation and stabilization, Chapter 5. Elsevier Applied Science, London
22. Peeling J, Clark DT (1981) J Appl Polym Sci 26:3761
23. Clodoaldo S, Maria IF (2004) Mater Sci Eng A370:293
24. Scoponi M, Ghiglione C (1997) Makromolecular Chemie 252:237
25. Allen NS, Mckellar JF (1979) Makromolecular Chemie 180:2875
26. Rivaton A, Morel P (1992) Polym Degrad Stab 35:131
27. Luengo C, Allen NS, Edge M, Wilkinson A, Parallada MD, Barrio JA, Santa VR (2006) Polym Degrad Stab 91:947
28. Wypych G (2003) Handbook of material weathering, 3rd edn. Chem Tec Publishing, Toronto and New York
29. The effect of UV light and weather on plastics and elastomers. Plastics Design Library a division of William Andrew Inc. USA: Norwich, 1994